MESH GENERATION FOR NUMERICAL SIMULATION OF FLUID-STRUCTURE INTERACTION WITHIN PROGRESSING CAVITY PUMPS

LIMA, João Alves de, jalima@dem.ufrn.br
PALADINO, Emilio Ernesto, emilio@dem.ufrn.br
ALMEIDA, Rairam Francelino Cunha de, rairamalmeida@gmail.com
ASSMANN, Felipe Pinheiro Mota, felipeassmann@interjato.com.br
PPGEM - Post-Graduate Program in Mechanical Engineering, Federal University of Rio Grande do Norte, 59072-970 - Natal - RN

Abstract. *Improving efficiency of pumping systems is one of the main industrial goals, mainly in extraction activities in the petroleum industry. The progressing cavity pump, shortly PCP, is a positive displacement pump used in artificial lift systems that has gained a strong attention, mainly because its ability of pumping high viscosity fluids with or without solid particles, as sand, for example. However, since it is a relatively new pumping system, few investigations of its hydrodynamic behavior, either numerical or experimental, are available. Most attempts to describe the PCP hydrodyanamics reveal use of simple models, normally considering steady state flow and/or simplified geometries, and models considering full 3D-unsteady hydrodynamics details of flow within PCPs were not found in literature. Therefore the present work is concerned with the generation of grids with optimized topologies to be used in computational simulations of flows inside PCPs, through total integration with the ANSYS/CFX package. The proposed mesh generation process, based on the PCP kinematic description, is fully justified in view of the great difficulties introduced by the PCP limiting geometric aspects, as well as the need to deal with high mesh deformations: for each time step simulation, large rotor moving boundary and dynamic mesh deformation must be taken into account. This intrinsic behavior made impossible, up to now, the computational flow simulation within a PCP, although the main commercial CFD packages (as ANSYS/CFX) has rencently made available automatic moving boundary and dynamic mesh deformation features. The main problem in using a commercial package is its inefficiency in handling automatic mesh deformation for large and cyclic displacements. In addition, with the present approach, use of automatic tetrahedrical mesh elements that suffer large linear and angular distortions (leading to negative volume elements) or manual input of better kinds of elements, as the hexahedrical ones, were avoided. The developed mesh generation method was implemented in Fortran 90 language, which can be employed as a dynamic linked library (BCP_MESHER.DLL) to run in ANSYS/CFX software or as a stand-alone software (BCP_MESHER.EXE). Finally, the present study should be extended for pumps with similar kinematic descriptions.*

Keywords*: Progressing Cavity Pump, 3D-Unsteady Computational Simulation, PCP Mesh Generation*

1. INTRODUCTION

Due to increasing difficulties to extract more viscous oils in ever deeper wells, improvement of artificial lift systems is a continuous technological task. A precise definition of the most adequate artificial lift system for a given well is still a hard challenge and, therefore, take into account the main features of the well is one of the best practices for a proper choice. Traditional mechanical pumping, gas-lift, centrifugal pumping, among others, are well-known artificial lift systems present in petroleum industry. The progressing cavity pump system (PCP, for short) is an artificial lift system based on the positive displacement concept that has recently gained strong attention, due main to its interesting ability to pump high viscosity fluids with or without solid particles, as sand, and, even, multiphase flows with high gas concentration. Furthermore, the PCP system has presented a higher efficiency than the rotor-dynamic pumping systems, translated into lower power consumption and lower initial investment. On the other hand, this efficiency is directly related to a sensible dynamic sealing ability among internal cavities, which characterizes the working principle of both metallic and elastomeric progressing cavity pumps. Therefore, in order to improve the efficiency of a PCP artificial lift system, deeper studies of the flow inside a PCP, more specifically, on the dynamic sealing region, are required.

Although experimental studies had been performed by the artificial lift group at Intevep/PDVSA (Méndez, 2002; Olivet, 2002; Olivet *et al*., 2002; Gamboa *et al*., 2002), the elevated and prohibitive costs involved in building an experimental setup lead researchers in this area to develop simplified and computational models as an alternative route to obtain technical information that could give more physical insight on PCPs flow dynamics. The most representative simplified models were developed by Gamboa *et al*. (2002) and Pessoa *et al*. (2009). In parallel, Andrade (2008) developed an interesting simplified model where the flow is solved between two plates, whose local separation corresponds to the distance between rotor and stator, using a an approach similar to the lubrication theory, where inertial terms are neglected in the transport equations but the transient term is retained. This model provides, with some limitations, some more physical information on flow inside metallic PCPs. Even though these simplified models could be used as excellent tools in producing input data for development of control algorithms of PCP operational conditions, due to their intrinsic simplifying nature, none of them is able to offer detailed physical information on flow dynamics, neither on fluid-structure interaction between rotor and stator, which is important in an elastomeric-stator PCP.

With regard to a fully computational approach, Gamboa (2000) had already tried to develop and run, unsuccessfully, a complete model for study of the flow dynamics on metallic PCPs, employing the commercial finite element-based software FIDAP 11. He attributed the unsuccessful model implementation to limitations of the CFD software to handle mesh motion/deformation and moving boundaries, combined with different helix angles present in this kind of pump, which distort the tetrahedral and hexahedral elements used for discretization of equations (see also Dall'Acqua, 2000; Gamboa *et al.*, 2002). Currently, with the inclusion of the immersed meshes concept, FEA and CFD softwares (ANSYS, 2009) are already handling some of these issues, although with some strong limitations, mainly for turbulent flow simulations.

Therefore, under this viewing, the present work proposes a fully-integrated ANSYS/CFX package methodology for automatic mesh generation for three-dimensional flow and structure dynamic simulations within progressing cavity pumps. The developed methodology can be implemented as a Fortran 90 dynamic linkage subroutine (BCP_MESHER.DLL) or as a stand-alone executable program (BCP_MESHER.EXE), being capable to dynamically generate meshes and connectivity matrices as the rotor moves inside the stator, in a totally compatible ANSYS/CFX format. This methodology can be used for all kinds of PCP, metallic or elastomeric, with or without interference between rotor and stator, and, certainly, will be extended for similar pumps.

2. METHODOLOGY

2.1. General Aspects

Initially, it was tried to impose the full movement of the rotor inside the PCP, through automatic prescription of the mesh displacement by CEL language (CFX Expression Language), starting from an initial mesh, previously built in ICEM/ANSYS mesh generation software (ANSYS, 2009). This approach requires specification of a stiffness parameter (displacement diffusion/mesh stiffness) that automatically governs subsequent mesh point displacements. It did not show to be adequate, since introduces mesh residual deformation that highly distorts the elements in successive time steps. This residual deformation is due to numerical errors in the solution of Poisson equation, used by numerical packages to update spatial coordinates of internal nodes.

Figure (1) illustrates this behavior, bringing snapshots of the fluid domain mesh in a transversal plane of the PCP for four different instants of rotor positions (RPM = 60).

(a) $t = 0\ s$

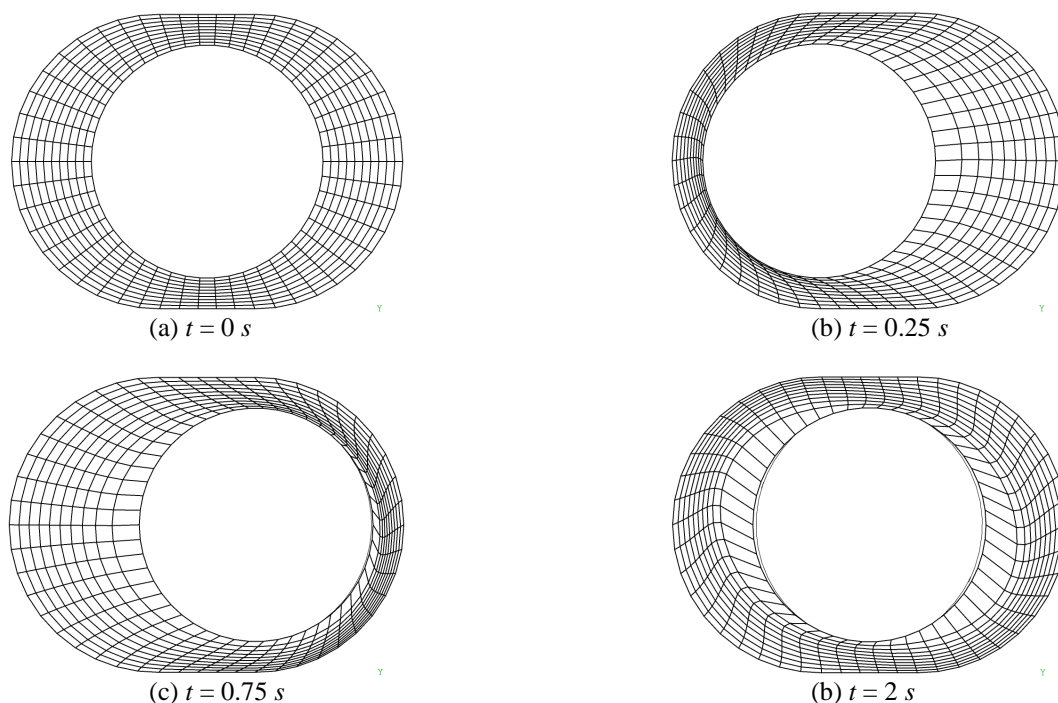(b) $t = 0.25\ s$

(c) $t = 0.75\ s$

(b) $t = 2\ s$

Figure 1. Mesh snapshots illustrating large distortions introduced with automatic
ANSYS/CFX mesh displacement procedure (using stiffness parameter)

Since the previous direct approach did not work properly, a procedure/subroutine was elaborated, based on the kinematics of the progressing cavity pumps, to dynamically evaluate, at any specified time, all mesh point coordinates and automatically establish the connectivity among all elements of the computational mesh, i.e., nodes, faces and element numbering, boundary conditions numbering and assembly of elements. Such connectivity is a requirement of

the ANSYS/CFX software, for consistency verification between initial and subsequent meshes, in order to keep the mesh topology along the time. In the ANSYS/CFX package, the mesh motion is imposed through the moving mesh algorithm (not by field interpolation in subsequent meshes) with the aim of maintaining the conservativeness and consistency of the numerical discretization. Then, elements are not suppressed or added in the domain, as rotor approaches to or retreats from the stator and the fluid velocity relative to the mesh velocity is considered for calculating the mass and momentum fluxes at control volumes faces in the discretization of the convective terms.

The connectivity matrix is obtained in a similar manner as implemented by the majority of the commercial packages, where the enumerating procedure that identify each element follows the right hand ruler for each face, with the unit normal vector pointing to the volume of the element (material). Thus, for the two right-handed coordinate systems illustrated in Fig. (2), enumeration first increases in the positive x direction, then increases in the positive y direction and, finally, in the positive z coordinate. This procedure must also be followed for elements enumerating.

(a)   (b)
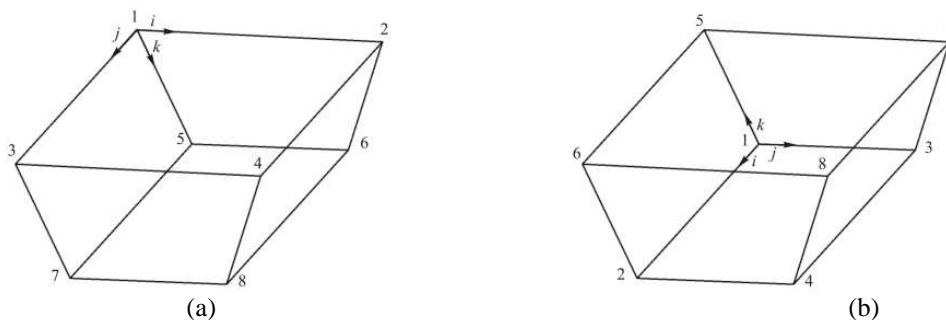
Figure 2. Node and element numbering procedure according to right hand ruler:
(a) downward normal vector, (b) upward normal vector

As is done in a typical CFX5 (and later versions) mesh file, physical node coordinates are firstly disposed in three increasingly ordered columns, according to x, y and z axis components, in a mesh file (BCP_FLUID.CFX5 and BCP_STRUCT.CFX5). The next part of the file shows element and node numbers, recorded according to the previous physical nodes arrangement. Finally, the patches for boundary conditions are identified by recording element and face numbers that characterizes the respective boundary surfaces. Once the present methodology is gaining more penetration in computational simulations, others types of mesh file formats, for use in other codes, will be made available, further spreading its usage.

As illustrated in Figs. (3), with the present approach it is possible to generate meshes for metallic or elastomeric pumps that present geometric characteristics with clearance (negative interference), null clearance/interference (perfect contact) and positive interference (only for elastomeric PCP) between rotor and stator. For null (perfect contact) and positive interference it assumed that a small liquid film is always present between rotor and stator in order to guarantee a single-connected fluid domain along the pump, without isolated cavities (which would represent a mathematical impossibility for the numerical method). The liquid film thickness is controlled through a user parameter that is made as small as possible, without committing the quality of the generated mesh.

(a)   (b)   (c)
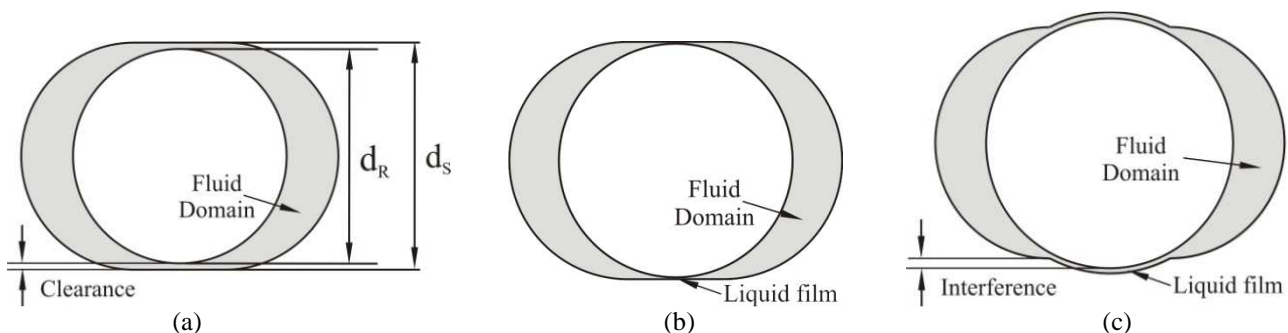
Figure 3. Types of geometry and mesh handled with the present approach. PCP/Mesh with:
(a) clearance or negative interference, (b) null interference/clearance, (c) positive interference

With the objective of minimize mesh distortions, and therefore, offer an optimized approach for mesh generation, four mesh configurations possibilities were studied, all of them guided by the cylindrical nature of the PCP system.

Initially, according to Figs. (4) and (5), for a transversal section of a PCP, meshes for fluid (in white) or solid/stator regions (not shown, but following the same topology) can be generated by tracing radial lines starting either from the rotor center (a "dynamic" mesh) or from the stator center (a "pseudo-static" mesh), respectively.
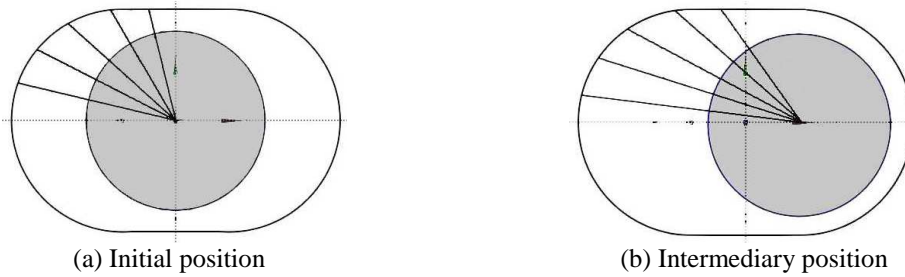
(a) Initial position (b) Intermediary position
Figure 4. Transversal mesh topology with rotor center as origin of the radial mesh lines:

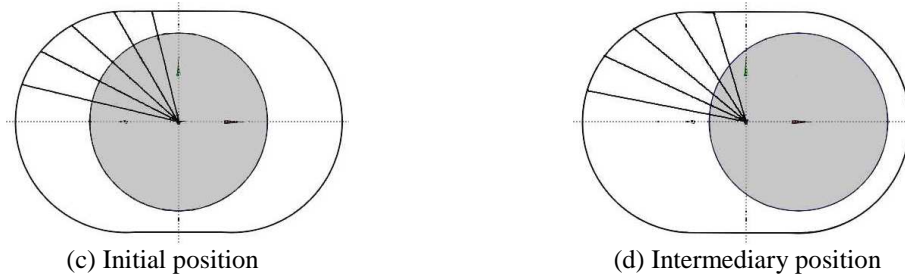(c) Initial position (d) Intermediary position
Figure 5. Transversal mesh topology with stator center as origin of the radial mesh lines

As can be seen on Figs. (6) and (7), with the last topology, where the origin of the planar mesh is fixed at the stator center, it is avoided large angular distortions, differently from the first one, where elements are naturally stretched as the rotor center moves periodically along the *x* axis.

This conclusion is better understood through a closer look on meshes generated with both topologies. Figures (6a) and (6b) illustrate the distorting effect on using the transversal mesh topology with rotor center as the origin of the radial mesh lines. Figure (7a) and (7b) illustrate the improvement obtained with the mesh topology where the stator center is the origin of the radial mesh lines.
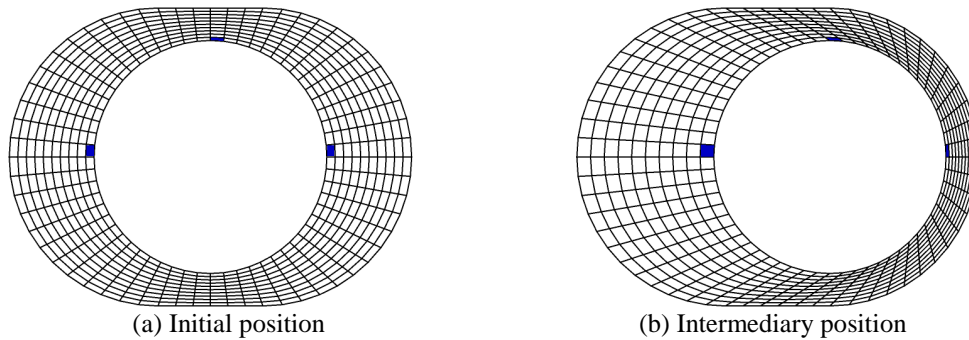

(a) Initial position (b) Intermediary position
Figure 6. Effect on mesh distortion for topology with rotor center as origin of the radial mesh lines

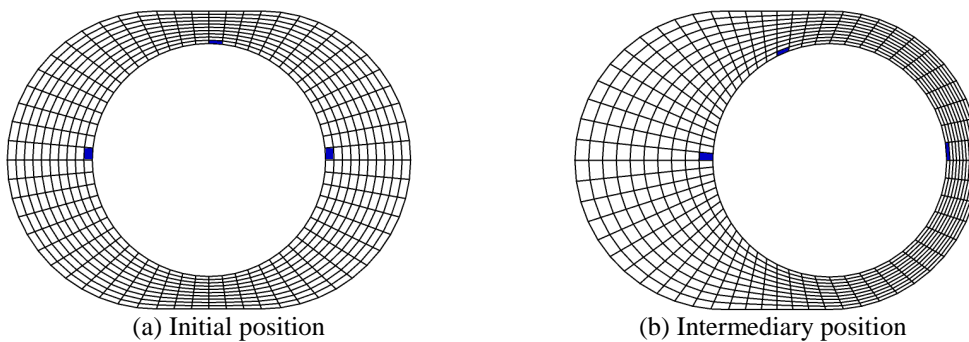

(a) Initial position (b) Intermediary position
Figure 7. Effect on mesh distortion for topology with stator center as origin of the radial mesh lines

It can be seen from these figures that the first topology introduces strong angular distortions on mesh as the rotor displaces. This behavior is not present in the last topology, where distortions are minimized and element orthogonality is preserved. Also, the last approach behaves as a "pseudo-immersed" mesh, since the mesh stays "static" while the rotor moves periodically.

Relative to longitudinal/axial mesh discretization, two possibilities were studied, for any of the previously defined transversal topologies. As it is done by the ANSYS/ICEM software, longitudinal lines can be traced following the solid generating lines that are created with the helical extrusion in the CAD solid builder, or can be simply straightly traced along the axial coordinate with no helical rotation. Figures (8a) and (8b) illustrate these two options.

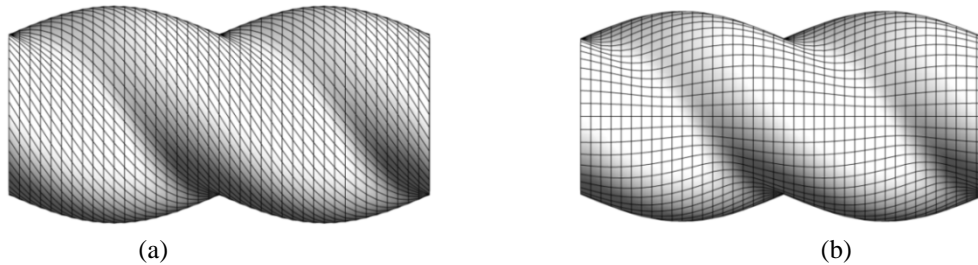(a)   (b)

Figure 8. Longitudinal mesh topology: (a) following helical construction lines, (b) following straight longitudinal lines

So far, it appears that the best topological configuration is obtained with a mesh generated from combination of the transversal topology of Fig. (5) with the longitudinal topology of Fig. (8b). Therefore, all results showed in the present work were obtained with this optimized mesh topology.

2.2. Mesh Generation Mathematical Description

First of all, in order to have a general approach for mesh generation, the mathematical equations that describe the kinematics of a PCP have to be determined. This is algebraically obtained for a single-lobe pump, starting from the sketch illustrated in Fig. (9). From this figure, the following main variables can be defined:
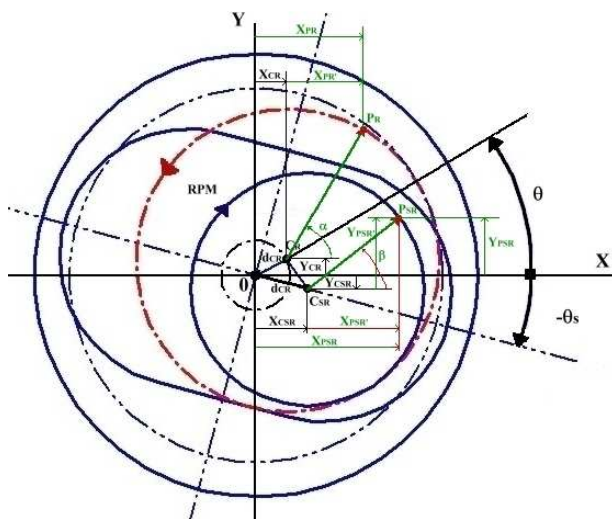
$$\theta_S = \frac{2\pi}{P_S} Z \tag{1}$$

$$\theta = \theta_0 + \omega t \tag{2}$$

$$\omega = \frac{2\pi}{60} RPM \tag{3}$$

$$d_{CR} = E \tag{4}$$

$$d_{CSR} = 2 E \cos(\theta - \theta_S) \tag{5}$$

Figure 9. Sketch illustrating the main variables involved in the kinematic of a PCP.

Where,

P_S	- Stator pitch
Z	- Longitudinal position/coordinate along the PCP
θ_S	- Stator angular position, related to the longitudinal position
θ_0	- Rotor initial angular position
θ	- Rotor angular position, related to its angular rotation
ω	- Rotor angular rotation
t	- Time instant
RPM	- Pump operational rotation
E	- Pump eccentricity
R_{SR}	- Radius of the rotor transversal section
d_{CR}	- Radius/displacement of the centerline rotor helix
d_{CSR}	- Displacement of the centerline rotor transversal section

Now, considering a transversal face Z_0 on pump and a radial line that forms an angle γ with the positive X axis, due to the helical nature of the rotor, a point P_0 (X_0, Y_0) on the rotor circumference centered at C_0, will be positioned in another transversal face Z (characterized by a stator angular rotation, θ_S) as point P_1 (X_1, Y_1) on the rotor circumference centered at C_1. This can be better visualized on Fig. (10).

Also, according to the (X, Y) coordinate system on this figure, coordinates of points P_0 (X_0, Y_0) and P_1 (X_1, Y_1) are written as:
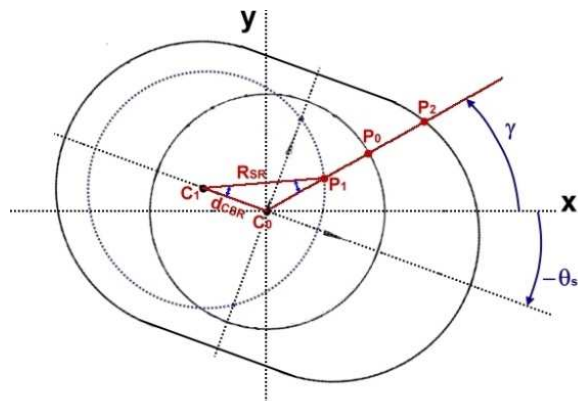
$$\begin{cases} X_{P0} = R_{SR}\cos(\gamma) \\ Y_{P0} = R_{SR}\cos(\gamma) \end{cases} \tag{6, 7}$$

$$\begin{cases} X_{P1} = X_{CSR} + R_{SR}\cos(\gamma + \gamma_{RT}) \\ Y_{P1} == Y_{CSR} + R_{SR}\sin(\gamma + \gamma_{RT}) \end{cases} \tag{8, 9}$$

Figure 10. Sketch illustrating position of transversal rotor sections as function of longitudinal coordinate Z

Whichever the topology employed, the computational mesh can be obtained through determination of the coordinates of the intersection between the radial straight lines with circumferences (rotor and circular part of the stator) or with straight lines (linear part of the stator), in association to a node/point insertion algorithm along the radial segment between these two intersection points. For a single-lobe PCP, this translates on:

- Line/Circumference Intersection: Nodes on rotor and on circular part of the stator

Radial Line Equation: $\quad y = Ax$; $\quad\quad A = \tan(\gamma)$ $\hspace{4cm}$ (13, 14)

Circumference Equation: $\quad (x - x_0)^2 + (y - y_0)^2 = R^2$ $\hspace{4cm}$ (15)

Substitution of one equation in another gives the following quadratic equation, whose solution is the spatial coordinate x of the intersection point. The coordinate y is automatically obtained from Eq. (13).

$$ax^2 + bx + c = 0, \quad \begin{cases} a = A^2 + 1 \\ b = -2(x_0 + Ay_0) \\ c = x_0^2 + y_0^2 - R^2 \end{cases} ; \quad x = \frac{-b \pm \sqrt{b^2 - 4ac}}{2a} \tag{16-18}$$

Depending on considering rotor or circular part of the stator, the following values have to be used:

$$\text{Rotor:} \begin{cases} x_0 = X_{CSR} \\ y_0 = Y_{CSR} \\ R = R_{SR} \end{cases} ; \quad\quad \text{Stator:} \begin{cases} x_0 = 2E\cos(\theta_S) \\ y_0 = 2E\cos(\theta_S) \\ R = R_{ST} \end{cases} \tag{19, 20}$$

- Line/Line Intersection: Nodes on straight lines of the stator

Radial Line Equation: $\quad y = Ax$; $\quad\quad A = \tan(\gamma)$ recalled from Eqs. (13) and (14)

Straight Lines Equation: $\quad y = Cx + D$; $\quad \begin{cases} C = \tan(\theta_S) \\ D = \pm \dfrac{R_{ST}}{\cos(\theta_S)} \end{cases}$ $\hspace{3cm}$ (21-23)

Substitution of one equation in another gives the following spatial coordinate x of the intersection point. The coordinate y is automatically obtained from Eq. (13).

$$x = \frac{D}{A - C} \tag{24}$$

Depending on longitudinal topology adopted, Fig. (8a) or Fig. (8b), the axial coordinate Z is obtained from Eq. (1) or incremented by a ΔZ longitudinal step, respectively. Also, depending on relative position between rotor and stator, special situations may produce singularities, which should be carefully observed on the code implementation phase.

Finally, since the final usage of the present methodology will be on FEA and CFD applications, where strong near walls gradients are always present, user has an additional setting parameter (*scale*) for near wall mesh refinement purposes, which take into account, simultaneously, the wall proximity of both rotor and stator. The following formula will be automatically applied for all coordinates points previously obtained:

$$(x, y)_T = 0.5 \left[1 + \tanh \left(2 \times scale \times (x, y) - scale \right) \right] \tag{25}$$

The advantages of the mesh density procedure can be understood from Figs. (11a) and (11b) which show two detailed views of two numerical mesh generated without (*scale* = 0) and with (*scale* = 1.5) use of the wall mesh density parameter, respectively. For CFD applications, mesh of Fig. (11b) will be more suitable. As one can realize, this is a valuable tool that, certainly, will be required for turbulent flow predictions. This near-wall mesh refinement further improves the present methodology for PCP mesh generation.
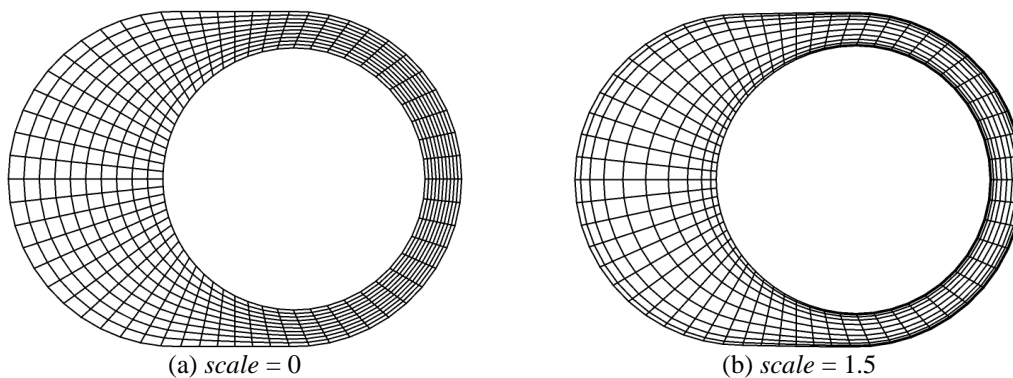

(a) *scale* = 0   (b) *scale* = 1.5

Figure 11. Near-wall grid refinement introduced with the contraction scale factor

3. RESULTS

The present methodology was implemented as a dynamically linkage library (*BCP_MESHER.DLL*), executed in real time with the ANSYS/CFX package, and as a stand-alone software (*BCP_MESHER.EXE*), for fast mesh viewing purposes. The following geometrical and mesh parameters (that characterize a PCP) have to be informed, as an input file for the DLL routine, or directly from the graphical interface of the executable program:

E	- eccentricity
RSR	- rotor transversal section radius
RST	- minor stator radius
RTUB	- internal pump/tube radius
PST	- stator pitch
NPST	- PCP number of pitches
NPL	- number of points along a circumferential line
NLZ	- number of concentric lines in a transversal face
NFZPST	- number of faces along longitudinal direction per PCP pitch
TETA0	- initial rotor angular position
WF	- tolerance for clearance hypothesis (liquid film)
WMIN/WMAX	- minimum/maximum deformation for a linearly deformable elastomeric pump stator
SCALE	- near-wall contraction mesh scale, defined by Eq. (25)

Figures (12a) and (12b) show, respectively, the graphical interface of the stand-alone program developed and its typical input file. For the graphical interface, additional options for mesh generation and execution, like topology and numerical precision choices are available. Parameters entered through the graphical interface can also be recorded as an input file for future use on the dynamic linkage library option.

After execution, a mesh output file is recorded containing all information about the mesh generated, such as superficial and volumetric nodes and elements numbers, among others.
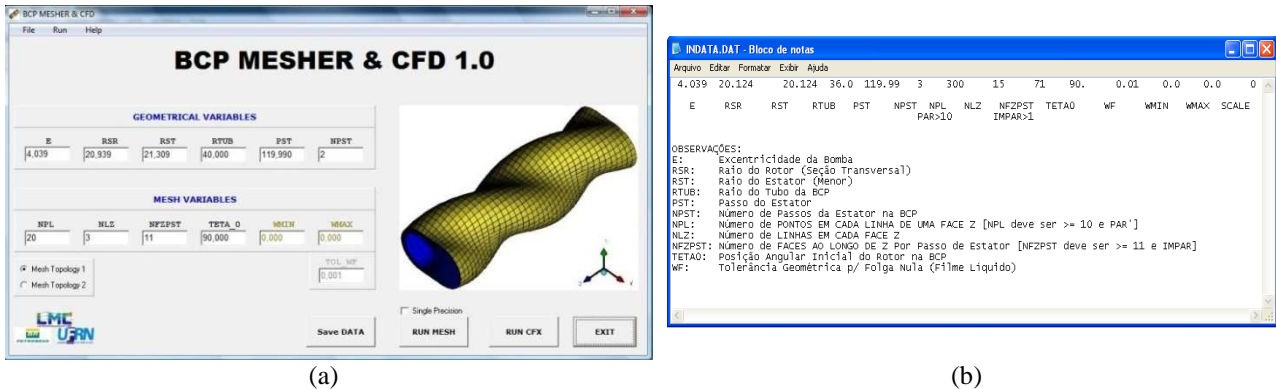

| (a) | (b) |

Figure 12. (a) Graphical interface of the developed software for PCP meshing, (b)Typical input file

Additional subroutines that allow communication of the present subroutine with the ANSYS/CFX kernel, through a memory management system for variables sharing - MMS, are provided together with the ANSYS/CFX package.

Figures (13) and (14) illustrate 3D patterns of meshes created with the present methodology, in grid and solid representations, for both types of longitudinal topologies. As one can see, the second topology yields the best approximation of purely hexahedral elements, with minimum angular distortion along z coordinate,
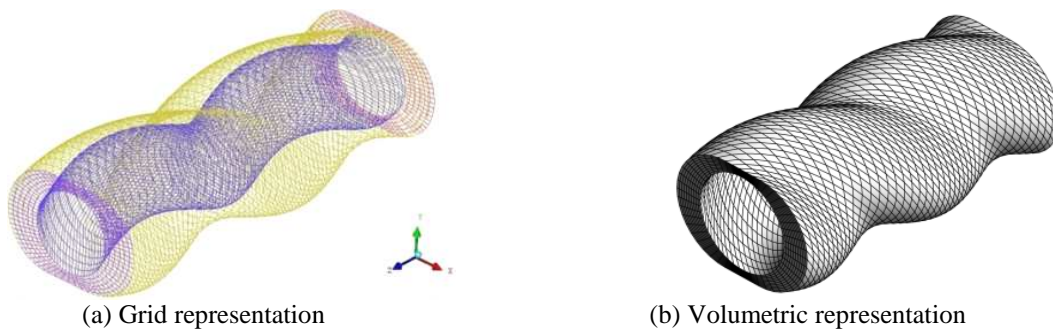

| (a) Grid representation | (b) Volumetric representation |

Figure 13. Numerical mesh representing the 3D PCP fluid region, topology based on helical construction lines

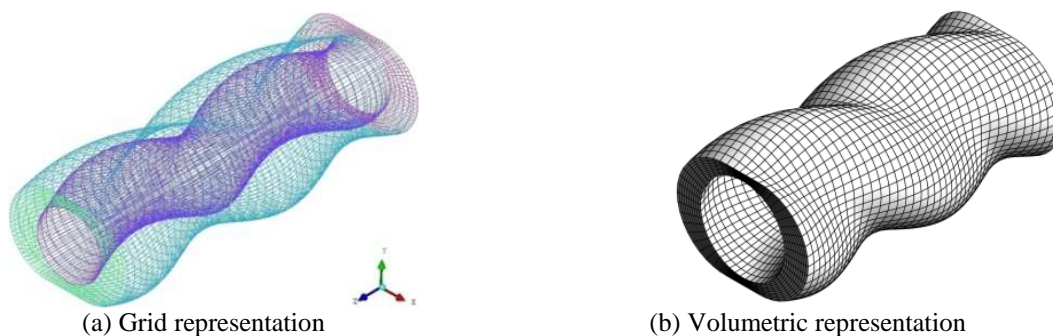| (a) Grid representation | (b) Volumetric representation |

Figure 14. Numerical mesh representing the 3D PCP fluid region, topology based on straight longitudinal lines

Now, in order to demonstrate the versatility of the present mesh generator, some mesh convergence studies and results for a typical PCP operating situation are illustrated. A more extensive description and validation of the CFD model is presented in Paladino *et al.* (2009).

Figures (15a) and (15b) bring illustrations of the details level provided by the present approach, after a post processing of results obtained for a typical situation from an ANSYS/CFX simulation.

Figure (15a) shows how dynamical longitudinal and transversal pressure profiles (pressure versus time) are easily plotted for any position on the pump, through probes placed at numerical nodes on grid. The longitudinal pressure distribution at the PCP stator surface is also easily visualized, showing how cavities are simultaneously strengthened while rotor is dynamically positioned.

Figure (15b) illustrates the dynamic behavior of the longitudinal and transversal slip flows between two consecutive cavities. The "slippage" between cavities plays the most important role on PCP efficiency definition.

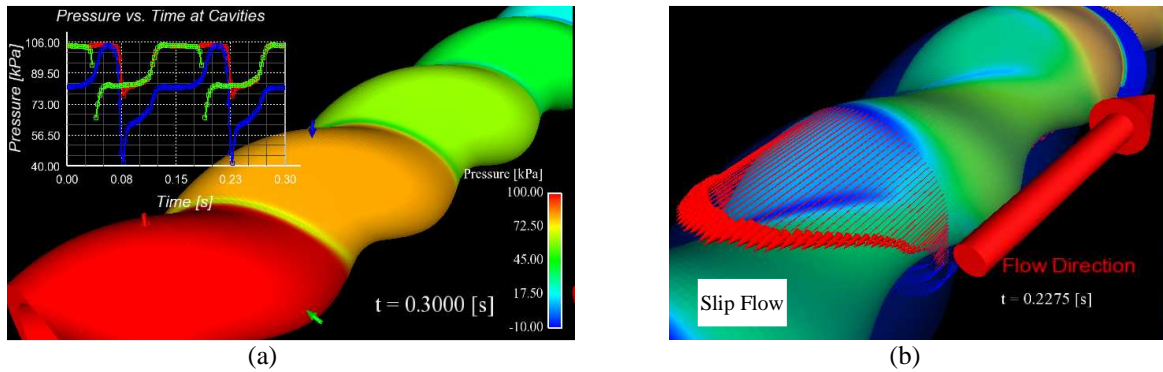(a)   (b)

Figure 15. (a) Pressure history for three probes and pressure contour along stator,
(b) Instantaneous longitudinal and transversal slip flows between cavities

Figure (16a) and (16b) offer more technical results, showing convergence analysis and comparison with experimental results, for validation purposes.

Figure (16a) brings the mass flow rate as a function of the global differential pressure applied on a PCP, by considering flow of two oils with viscosity 42 cp and 481 cp, for a pump operating at 200 RPM. Results are compared against the experimental results of Gamboa *et al*. (2002). The experimental data are completely reproduced for both fluids, validating the proposed mesh generation algorithm. As expected, the decreasing in mass flow rate behavior for increasing differential pressure, which follows directly from the gradual slip flow among cavities, mainly for low viscosity oils, is achieved by the present approach.

Figure (16b) brings the convergence analysis for the flow of the 42 cp oil, at a differential pressure of 40 psi. At least for engineering purposes, results are already fully converged by employing a numerical mesh with 10^6 nodes.

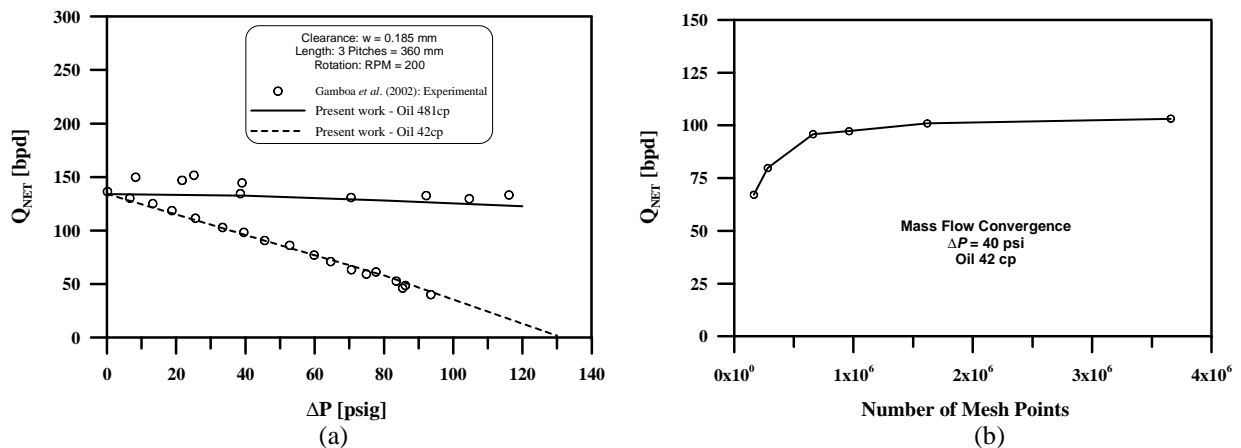(a)   (b)

Figure 16. (a) Mass flow rate behavior as function of the PCP global differential pressure,
(b) Convergence analysis for the mass flow rate

Finally, a complete historic of the development of the present methodology can be found in a series of technical reports and presentations sent to Petrobras by the computational simulation group at LMC/UFRN (Lima and Paladino, 2006a, 2006b, 2007a, 2007b, 2008a, 2008b; Lima *et al.*, 2009). Recently, research is being developed with the objective of study the truly fluid-structure interaction, by considering PCP with elastomeric stator deformation. The structural behavior of the elastomer is introduced in the ANSYS package through definition of constitutive models for rubbers.

4. CONCLUSION

So far, none full computational simulation of the PCP dynamics had been effectuated, since even the new philosophy of immersed meshes did not prove to be adequate for this kind of geometry. However, the proposed computational mesh methodology (automatic mesh generation, via DLL Fortran routine, with further running in execution time, through ANSYS/CFX Junction Box option) showed to be an adequate computational strategy for simulations of fluid-structure interaction within progressing cavity pumps. With only initial geometric and operational input parameters, three-dimensional flow and structural dynamic behaviors within a PCP are entirely performed by the ANSYS/CFX package without any other user interference. In addition, the study of several topological possibilities has made possible to find the most optimized mesh configuration for simulation purposes.

From a specific point of view, the following advantages can be listed with the development of the present mesh generation methodology for PCP simulation:

- No need of solid models generation in CAD software as SolidEde, SolidWorks or DesignModeler, since the geometry is entirely represented by mesh description.

- No need of use of ICEM/ANSYS package, or similar, for hexahedral meshes generation.

- Automatic generation of meshes for any geometric parameters modification. Again, this characteristic evidences the advantage of avoiding the two previous phases.

- Null clearance and even positive interference situations can be easily performed by introducing a small clearance parameter, which can be adjusted depending on the pressure gradient along the pump.

- Full integration with the ANSYS/CFX package. All communication with the ANSYS/CFX software is done automatically, without user interference.

- Finally, it should be pointed out that the present 3D-unsteady computational approach can be easily extended for similar pumps that share the same kinematic principles.

5. ACKNOWLEDGEMENTS

6. REFERENCES

Andrade, S.F.A., 2008, "Asymptotic Model for Monophasic Flow through Progressive Cavities Pump", Ms.C. Thesis (in portuguese), PUC/RJ, Rio de Janeiro, Brazil, 116 p.

ANSYS Inc., 2009, "Reference and Theory Manual", USA.

Dall'Acqua, D., 2000, "Thermo-mechanical Modelling of Progressing Cavity Pumps and Positive Displacement Motors", MSc. Thesis, University of Alberta, Edmonton, Canada.

Gamboa, J.A.B., 2000, "Computational Simulation of a PCP with no Interference", Mc.S. Thesis (in spanish), Universidad Simón Bolívar, Sartenejas, Venezuela.

Gamboa, J.A.B; Olivet, A.J.S.; González, P. And Iglesias, J., 2002, "Understanding the Performance of a Progressive Cavity Pump with a Metallic Sator", Proceedings of the 20th International Pump Users Symposium, USA.

Lima, J.A. and Paladino, E.E., 2006a, "Computational Simulation of the Fluid-Structure Interaction within PCPs" (in portuguese), Technical Report 1, May/2006, LMC/PPGEM/UFRN, Brazil.

Lima, J.A. and Paladino, E.E., 2006b, "Computational Simulation of the Fluid-Structure Interaction within PCPs" (in portuguese), Technical Report 2, December/2006, LMC/PPGEM/UFRN, Brazil.

Lima, J.A. and Paladino, E.E., 2007a, "Computational Simulation of the Fluid-Structure Interaction within PCPs" (in portuguese), Technical Report 3, July/2007, LMC/PPGEM/UFRN, Brazil.

Lima, J.A. and Paladino, E.E., 2007b, "Computational Simulation of the Fluid-Structure Interaction within PCPs" (in portuguese), Technical Report 4, December/2007, LMC/PPGEM/UFRN, Brazil.

Lima, J.A. and Paladino, E.E., 2008a, "Computational Simulation of the Fluid-Structure Interaction within PCPs" (in portuguese), Technical Report 5, June/2008, LMC/PPGEM/UFRN, Brazil.

Lima, J.A. and Paladino, E.E., 2008b, "Computational Simulation of the Fluid-Structure Interaction within PCPs" (in portuguese), Powerpoint Presentation at Petrobras/Cenpes, October/2008, LMC/PPGEM/UFRN, Brazil.

Lima, J.A., Paladino, E.E., Almeida R.F.C., Pessoa, P.A.S., Assmann, F.P.M., Assmann, B.W., 2009, "Computational Simulation of the Fluid-Structure Interaction within PCPs" (in portuguese), Final Technical Report, June/2009, LMC/PPGEM/UFRN, Brazil.

Méndez, R.J., 2002, "Experimental Study of Temperature Effect on Efficience of a Progressing Cavity Pump", Mc.S. Thesis (in spanish), Universidad Simón Bolívar, Sartenejas, Venezuela.

Olivet, A.J.S., 2002, "Experimental Study of the Efficiency of a Metallic PCP with Two-Phase Flow", Mc.S. Thesis (in spanish), Universidad Simón Bolívar, Sartenejas, Venezuela.

Olivet, A.J.S.; Gamboa, J.A.B. and Kenyery, F., 2002, "Experimental Study of Two-Phase Pumping in a Progressive Cavity Pump Metal to Metal", SPE 77730 paper, SPE Annual Technical Conference and Exhibition, San Antonio, Texas, 29 September-2 October, USA.

Paladino, E.E., Lima, J.A., Pessoa, P.A.S. and Almeida R.F.C., 2009, "Computational 3D Simulation of the Flow within Progressive Cavity Pumps", Proceedings of the Brazilian Congress of Mechanical Engineering - COBEM 2009, Gramado, Nov. 15-20, Brazil.

Pessoa, P.A.S., Paladino, E.E. and Lima, J.A., 2009, "Simplified Model for the Flow in a Progressive Cavity Pump", Proceedings of the Brazilian Congress of Mechanical Engineering - COBEM 2009, Gramado, Nov. 15-20, Brazil.

7. RESPONSIBILITY NOTICE

The authors are the only responsible for the printed material included in this paper.